Mechanistic Insights into C2 and C3 Product Generation using Ni_3Al and Ni_3Ga Electrocatalysts for CO_2 Reduction

Aubrey R. Paris*, Andrew B. Bocarsly
Department of Chemistry, Princeton University, Princeton, New Jersey 08544, USA

*Correspondence: aparis@princeton.edu

Abstract

Thin films of Ni_3Al and Ni_3Ga on carbon solid supports have been shown to generate multi-carbon products in electrochemical CO_2 reduction, an activity profile that, until recently, was ascribed exclusively to Cu-based catalysts. This catalytic behavior has introduced questions regarding the role of each metal, as well as other system components, during CO_2 reduction. Here, the significance of electrode structure and solid support choice in determining higher- versus lower-order reduction products is explored, and the commonly invoked Fischer-Tropsch-type mechanism of CO_2 reduction to multi-carbon products is indirectly probed. Electrochemical studies of both intermetallic and non-mixed Ni-Group 13 catalyst films suggest that intermetallic character is required to achieve C2 and C3 products irrespective of carbon support choice, negating the possibility of separate metal sites performing distinct yet complementary roles in CO_2 reduction. Furthermore, Ni_3Al and Ni_3Ga were shown to be incapable of generating higher-order reduction products in D_2O, suggesting a departure from accepted mechanisms for CO_2 reduction on Cu. Additional routes to multi-carbon products may therefore be accessible when developing intermetallic catalysts for CO_2 electroreduction.

One-sentence summary (maximum 20 words): Systematic variations in catalyst structure and electrolyte isotopic labeling narrow down mechanistic possibilities for CO_2 reduction using Ni-Group 13 electrocatalysts.

Introduction

As atmospheric CO_2 becomes an increasingly significant global challenge, the development of efficient and selective electrocatalysts active in CO_2 reduction draws continuous attention. One goal for these catalysts is finding ways to generate higher-order, highly reduced products, effectively constructing C–C bonds from CO_2 subunits. Unfortunately, catalysts capable of electrochemically transforming CO_2 into multi-carbon products are rare; aside from Cu, bimetallic species have shown the greatest promise in this area.[1–3]

Models[4–6] and even machine learning algorithms[7,8] have been implemented to guide prediction of new bimetallic catalysts capable of reducing CO_2. Many of these calculations incorporate factors such as thermodynamic requirements for reduction of a CO intermediate, likelihood of surface restructuring, impact of exposed crystal faces, and scaling relations between the adsorption energies for CO and protonated reduction intermediates.[9] While these factors are important, other characteristics of both mono- and bimetallic systems, such as catalyst morphology,[10–13] spatial arrangement of the component metals,[14,15] and solid support material,[16] have been shown experimentally to impact product distribution, selectivity, and efficiency. Furthermore, an understanding of mechanisms employed by bimetallic systems—beyond the identification of a common CO intermediate—is lacking. Modeling, machine learning, and overall electrode design could be better informed by systematically exploring these catalytic factors, particularly for bimetallic species that are or may be capable of generating multi-carbon reduction products.

One class of CO_2-reducing bimetallic catalysts that benefits from such an analysis is comprised of Ni-Group 13 (i.e., Ni-G13) intermetallics. Thin films of Ni_3Al[3] and several Ni_aGa_b species (e.g., NiGa, Ni_3Ga, Ni_5Ga_3)[1,16] supported on carbon have drawn interest due to their unusual ability to electrochemically reduce CO_2 to C2 and C3 products, including 1-propanol, acetone, ethane, and ethanol. While the multi-carbon nature of these products might suggest a mechanism similar to Cu-mediated CO_2 reduction, the true means by which Ni-G13 materials facilitate C–C bond formation is largely unknown. Questions remain regarding the role of each metal in catalysis, such as whether the electrocatalytic layer is composed of an intermetallic compound or two separate metal phases. Further questions include the impact of factors such as carbon support and whether a mechanism resembling Fischer-Tropsch chemistry—often suggested for Cu catalysts[17–19]—is at work. A better understanding of these factors in the context of Ni-G13 catalysts could aid in the prediction and development of additional non-Cu-containing electrocatalysts having the ability to promote C–C bond formation.

Here, we study Ni_3Al on glassy carbon (i.e., Ni_3Al/GC) and Ni_3Ga on highly oriented pyrolytic graphite (i.e., Ni_3Ga/HOPG) to determine the influence of electrode structure (i.e., intermetallic compounds versus non-mixed metals; choice of solid support) in achieving multi-carbon products during CO_2 electroreduction. Our results support the importance of intermetallic character in attaining the desired multi-carbon products, suggesting that the individual metal components are not facilitating separate, stepwise reduction events en route to C–C bonds. Furthermore, the likelihood of C2 and C3 product formation via a Fischer-Tropsch-like process is indirectly assessed via experiments altering the isotopic composition of the electrolyte. In the end, the data reported herein raise questions as to whether Ni-G13 electrocatalysts utilize this commonly invoked mechanism, indicating that another pathway may be possible for achieving Cu-like products on non-Cu-containing catalysts.

Experimental

Ni_3Al and Ni_3Ga were prepared on glassy carbon (GC), highly oriented pyrolytic graphite (HOPG), and reticulated vitreous carbon (RVC) solid supports as described previously via the thermal reduction of metal nitrate salts under forming gas atmosphere.[1,3,16] Non-mixed samples (i.e., 3Ni-Al and 3Ni-Ga) were synthesized in an identical fashion, except the precursor metal nitrate solutions were not combined prior to drop-casting. Instead, thin strands of paraffin wax were wound tightly around the center of the carbon support to create a ~3 mm-high physical barrier separating the support into halves; the Ni(II) and Al(III) or Ga(III) nitrate solutions were then drop-casted on separate sides of the barrier while maintaining an overall 3:1 ratio of metals. The paraffin was removed prior to furnace treatment to generate a surface interface where a Ni salt was juxtaposed with either an Al or Ga salt.

Materials characterization was performed to confirm that the Ni_3Al and Ni_3Ga intermetallic species were formed in the mixed salt samples, as well as to verify that the metals had remained isolated in the non-mixed samples. The catalyst material was analyzed by powder X-ray diffraction (XRD), following careful removal of the films from their carbon supports, using a Bruker D8 Advance diffractometer with 0.083° step size and CuKα radiation. Surface compositions of the intact electrodes were examined by X-ray photoelectron spectroscopy (XPS) using a ThermoFisher K-Alpha instrument with 20 eV pass energy and 50 ms dwell time. XPS spectra were analyzed with the Thermo Scientific Avantage Data System and CasaXPS software. All peaks were referenced to adventitious carbon at 284.8 eV. Scanning electron microscopy (SEM) images were obtained using a FEI XL30 FEG-SEM equipped with an EVEX EDS detector for acquisition of XRD-complementing energy-dispersive X-ray spectroscopy (EDX) data. SEM and EDX data were collected using a 5 keV electron beam and ~12 mm working distance.

Electrolysis experiments were set up by fitting the working electrode, Ag/AgCl reference electrode, and Pt mesh counter electrode (within a gas dispersion tube) into the gas-tight ports of a custom electrochemical cell. As previously described,[3,16] the film-on-carbon working electrode was held using an alligator clip attached to Cu wire, which was threaded through a glass tube sealed with insulating epoxy. The electrolyte, stirred during experimentation, consisted of 0.1 M K_2SO_4 (in H_2O or D_2O, depending on experiment) buffered with $KHCO_3$ to achieve desired pH values following CO_2 saturation. Electrolyses were conducted using CH Instruments 760 and 1140 potentiostats until 50 coulombs of charge had passed, and measurements following these experiments failed to yield significant changes in solution pH.

Product analysis was accomplished by sampling the headspace and electrolyte by gas chromatography and ^{1}H-NMR spectroscopy, respectively. CO and ethane were detected using a HP6890 Gas Chromatograph with Molsieve 5A PLOT capillary column (Agilent), thermal conductivity detector (TCD), and He flow gas. H_2 was detected using an SRI 8610C Gas Chromatograph with Molsieve column, TCD, and Ar flow gas. Liquid products were analyzed using a Bruker Avance III 500 MHz NMR Spectrometer with a cryoprobe detector. A custom water suppression method permitted direct sampling of electrolyte solutions upon addition of 10 µL 1,4-dioxane (10 mM) as an internal standard. $^{13}CO_2$ control electrolyses were performed for newly reported catalyst species to confirm product derivation from CO_2, indicated by either peak splitting in the ^{1}H-NMR or gas-phase infrared spectroscopy. H_2 quantification confirmed charge balance in each experiment discussed herein.

Results and Discussion

Whether a heterogeneous, bimetallic CO_2 reduction catalyst consists of an intermetallic species or, more simply, two metals existing in the same electrochemical cell is influenced by the catalytic role of each metal. For example, considering a binary metal catalyst A-B, if metal A reduces CO_2 to CO and metal B selectively reduces CO to a multi-carbon final product, then a heterogeneous mixture of A and B would be expected to perform the catalytic task, while an intermetallic or alloy phase, AB, would potentially effect a different chemistry and product distribution. By association, determining whether the function of a two-metal catalyst depends on alloying could lend insight into the mechanism of CO_2 reduction on bimetallic species. In the case of Ni_3Al/GC and Ni_3Ga/HOPG, it is instructive to know whether generation of multi-carbon products is predicated on the presence of an intermetallic compound, as well as what this might mean for the mechanism underlying these catalysts' unique activities.

To examine the importance of electrode structure for these thin film Ni-G13 catalysts, intermetallic and non-mixed electrodes were prepared using a consistent synthetic method based on drop-casting and subsequent heat treatment.[1,16,3] Synthesis of the non-mixed electrodes, referred to as 3Ni-Al/GC and 3Ni-Ga/HOPG, differed from the Ni_3Al/GC and Ni_3Ga/HOPG intermetallic species in that the two constituent metals were isolated on the same carbon solid support. This prevented alloying during heat treatment yet permitted drop-casting of the same 3:1 Ni:G13 stoichiometry featured in the intermetallic films.

The materials characterization of Ni_3Al/GC[3] and Ni_3Ga/HOPG,[1,16] thin films having homogeneous compositions, has been reported previously. As shown in Figure S1, the non-mixed 3Ni-Al/GC and 3Ni-Ga/HOPG electrodes were striped, as each metal component occupied a distinct portion of the carbon support. Surface characterization data for 3Ni-Al/GC and 3Ni-Ga/HOPG are provided in Figures 1 and 2, respectively. X-ray photoelectron spectroscopy (XPS) suggests that, much like the parent intermetallics, the surfaces of the Ni, Al, and Ga stripes were either heavily or entirely oxidized. Furthermore, scanning electron microscopy (SEM) of the non-mixed metals showed that, on GC, both stripes were comprised of flat platelets, while the stripes on HOPG were rougher and less uniform in shape. This morphological distribution based on carbon solid support has been reported.[16] A complete

summary of characterization data comparing the non-mixed 3Ni-Al/GC and 3Ni-Ga/HOPG electrodes with their parent intermetallics is provided in Table 1.

The electrocatalytic performance of 3Ni-Al/GC and 3Ni-Ga/HOPG was compared to Ni_3Al/GC and Ni_3Ga/HOPG using CO_2 electrolysis experiments conducted at –1.38 V vs. Ag/AgCl, the potential previously shown to be optimal for CO_2 reduction mediated by the intermetallic species.[3,16] Electrolyses were conducted in two-compartment cells using CO_2-saturated, pH 4.5 K_2SO_4 (0.1 M) as the electrolyte and Pt mesh as the counter electrode. Figure 3 shows the product distribution achieved using 3Ni-Al/GC and 3Ni-Ga/HOPG alongside that of Ni_3Al/GC and Ni_3Ga/HOPG. While Ni_3Al/GC electrochemically reduces CO_2 to form a significant quantity of CO alongside 1-propanol, methanol, and even small amounts of ethanol and acetone,[3] the non-mixed 3Ni-Al/GC electrode only generated small quantities of CO and formate. Similarly, Ni_3Ga/HOPG's small Faradaic efficiency for ethane[16] is supplanted by an even smaller quantity of formate when using 3Ni-Ga/HOPG. In these and all subsequent experiments, H_2 generation was shown to account for the remaining charge (Figure S2).

Aside from indicating that, for these Ni-G13 catalysts, intermetallic character is required to achieve higher-order products from CO_2, these electrolysis experiments begin to answer a standing question about how Ni-G13 species facilitate CO_2 reduction. If the Ni and G13 metals had separate roles—facilitating discrete tasks in the stepwise reduction of CO_2 to multi-carbon species—one would have expected to generate the multi-carbon products even without alloying of the metals, since both metals would have been available to fulfill their respective roles. This assertion is further supported by experiments in which Ni/GC, Al/GC, Ni/HOPG, and Ga/HOPG were synthesized separately, mixed to homogeneity in appropriate 3:1 ratios post-furnace treatment, and reapplied to either GC or HOPG prior to electrochemical testing. These scenarios, in which the two metals were in direct, adjacent contact yet were not alloyed, still failed to yield higher-order products. Finally, while surface oxides are consistently present, Table 1 shows that the surface compositions of the intermetallic and non-mixed electrodes are nearly identical, so surface oxides cannot explain the differences in catalytic activity. These observations lead to the conclusion that Ni and G13 metals interact synergistically, rather than simply perform complementary tasks, in the CO_2 electroreduction process.

We previously reported that the Ni_3Ga intermetallic system exhibits a solid support dependence during electrochemical CO_2 reduction. Namely, choice of carbon support was shown to impact product distribution and CO_2 reduction pathway, which was largely attributed to surface character and morphology.[16] This phenomenon introduces the question of whether a solid support dependence might exist for non-mixed Ni-G13 electrocatalysts; one might hypothesize that the ability to generate higher-order products using non-mixed Ni-G13 electrodes might be reinstated by selecting an appropriate support material. Before examining this possibility using the Ni-G13 class of catalysts, it was first necessary to determine whether the product distribution obtained using the Ni_3Al intermetallic relies on solid support choice like the Ni_3Ga analog.

With its product distribution on GC well-characterized,[3] Ni_3Al was synthesized on HOPG and a third support material, reticulated vitreous carbon (RVC; structurally related to GC[20,21]), comprising the three electrode materials previously tested in the Ni_3Ga study. As shown in Figure 4, XRD analysis indicates that the desired intermetallic compound was synthesized on both carbons, while the morphologies of Ni_3Al/HOPG and Ni_3Al/RVC were consistent with those achieved for Ni_3Ga on the same supports. Specifically, Ni_3Al/RVC was comprised of smooth, platelet structures distributed across the porous carbon framework, whereas Ni_3Al/HOPG's morphology resembled that of 3Ni-Ga/HOPG discussed earlier. XPS analysis of the intermetallic surfaces revealed a likeness to Ni_3Al/GC, as surface-confined Al was comprised of Al_2O_3 and Ni was predominantly—or, in the case of Ni_3Al/RVC, entirely—oxidized prior to CO_2 electrolysis (Figures S3, S4).

Electrolysis experiments with Ni_3Al/RVC and Ni_3Al/HOPG electrodes were performed at –1.38 V vs. Ag/AgCl in pH 4.5, CO_2-saturated K_2SO_4 electrolyte. The results of these experiments, compared to the outcomes achieved using the GC-deposited species, are shown in Figure 5. While differences in product Faradaic efficiency are recorded for each solid support, the same major reaction products (i.e., CO, 1-propanol, methanol, and formate) are observed in all cases, indicating no change in product distribution. This result is distinctly different than what has been observed using Ni_3Ga on various carbons, which yields ethane on HOPG and CO, formate, and trace amounts of methanol on GC and RVC.[16] Because Ni_3Al does not exhibit solid support dependence in the intermetallic structure, it was not examined further for this dependence in the non-mixed 3Ni-Al form.

However, given the influence of solid support on product distribution attained using Ni_3Ga, the non-mixed 3Ni-Ga analog was prepared and tested on both GC and RVC. This would allow for comparison with 3Ni-Ga/HOPG examined earlier, as well as the intermetallic species Ni_3Ga/GC and Ni_3Ga/RVC discussed in our previously published work.[16] Complete materials characterization of Ni_3Ga/GC has already been reported, while additional details regarding Ni_3Ga/RVC, indicating similar bulk and surface compositions as the GC variant, are provided in Figure S5. Unsurprisingly, characterization revealed that the Ni half of 3Ni-Ga/GC was compositionally and morphologically identical to the Ni half of 3Ni-Al/GC depicted in Figure 1. For completeness, XRD, XPS, and SEM data for the Ga half of 3Ni-Ga/GC and both halves of 3Ni-Ga/RVC are shown in Figures S6 and S7. As was the case for Ni on GC and HOPG, the Ni stripe on RVC was comprised of metallic Ni in the bulk, while the surface featured a mixture of metal and oxides. The Ga stripes on both GC and RVC consisted of monoclinic Ga_2O_3 and were predominantly oxidized at the surface, as well.

Figure 6 gives the results of 3Ni-Ga/GC and 3Ni-Ga/RVC electrolysis experiments, performed at –1.38 V vs. Ag/AgCl in pH 4.5, CO_2-saturated K_2SO_4, alongside the previously reported results for Ni_3Ga on these solid supports. 3Ni-Ga/GC and 3Ni-Ga/RVC both generated CO as their major product and small amounts of formate and methanol in the liquid phase, in accordance with the product distribution of their intermetallic counterparts. In short, altering the carbon used to support non-mixed Ni and Ga failed to reintroduce the ability to generate higher-order products, an outcome that remains reliant on intermetallic character.

Despite a lack of multi-carbon products, a noteworthy outcome achieved while examining 3Ni-Ga/RVC electrodes is their high Faradaic efficiency for CO (~52%). To further investigate this result, control electrolyses were performed using electrodes prepared by drop-casting either Ni or Ga onto each carbon support material; resulting Faradaic efficiencies for CO, formate, and methanol are listed in Table S1. In these experiments, the greatest quantity of CO was produced by the nominal Ga/RVC electrode (actual composition = monoclinic Ga_2O_3/RVC) at ~57% Faradaic efficiency (Figure S8), outcompeting H_2 evolution. Potential and pH dependence studies using Ga/RVC electrodes suggest that significant quantities of CO can be generated across a range of electrochemical conditions (Figure S9). This observation merits noting, as literature reports of Ga and Ga_2O_3's activity in CO_2 electroreduction are limited. In 1994, Hori *et al.* reported that a Ga electrode could generate CO at 23% Faradaic efficiency at –1.45 V vs. Ag/AgCl in neutral solution,[22] while a more recent report stated that Sn- or Si-doped Ga_2O_3 single crystals could reach >80% Faradaic efficiency for formate at potentials more negative than –1.8 V vs. Ag/AgCl.[23] As such, when considering a combination of Faradaic efficiency, overpotential, and chemical stability (Figure S10), the monoclinic Ga_2O_3 film on RVC examined here expands—and perhaps improves—upon previous reports of Ga species facilitating two-electron CO_2 reduction to form CO.

In any case, a common feature of the most interesting catalyst species studied here (i.e., Ni_3Al/GC and Ni_3Ga/HOPG, which make multi-carbon products, and Ga/RVC, whose CO_2 reduction rivals H^+ reduction) is CO generation capacity. Ga/RVC produces CO at high Faradaic efficiencies, while previous reports show that Ni_3Al/GC and Ni_3Ga/HOPG invoke CO as an

intermediate en route to higher-order products.[1,3,16] With this in mind, many researchers describe CO_2 electroreduction to highly reduced products, facilitated by Cu-based systems, as a mechanistically Fischer-Tropsch-type process,[21–23] though specific C2 products (e.g., ethylene) have been attributed to different pathways.[24,25] The mechanism by which Ni-G13 intermetallics generate C–C-bonded products is less well understood. A good first approximation might be determining whether their mechanistic pathways are Fischer-Tropsch-like in nature, thereby testing the prediction that their mechanisms resemble Cu-mediated catalysis.

Fischer-Tropsch catalysis has long been known to exhibit isotope effects when substituting H_2, the key reactant alongside CO, with D_2.[26] To determine whether Ni_3Al/GC or Ni_3Ga/HOPG demonstrate a similar effect, electrolysis experiments were conducted in D_2O (0.1 M K_2SO_4). Faradaic efficiencies for CO, obtained at an operating potential of –1.38 V vs. Ag/AgCl, are summarized in Figure 7, which also includes data obtained using Ni_3Ga/GC (i.e., an intermetallic that generates a modest amount of CO instead of multi-carbon products) and Ga/RVC (i.e., a single-metal species that generates a large amount of CO) for comparison. CO production increases in the presence of D_2O on all catalyst species studied, reaching 80% on Ga/RVC. Importantly, Ni_3Al/GC and Ni_3Ga/HOPG fail to generate their higher-order reduction products in D_2O despite the high relative abundance of CO, which serves as the intermediate en route to C2 and C3 products on these electrodes in H_2O-based electrolytes. In fact, Ni_3Ga/HOPG in H_2O has been shown to reduce CO to ethane, and in these experiments CO is usually present only in trace quantities during CO_2 reduction[1,16]; in the D_2O experiment described here, CO is quantifiable.

Substituting D_2O for H_2O in these electrochemical systems is clearly debilitating to the Cu-like behavior of Ni-G13 catalysts. In the presence of D_2O, the sustained generation of CO coupled with an inability to reduce it further suggests that CO reduction is rate-limiting, refuting the hypothesis made in our first report on the Ni_3Al/GC system.[4] Furthermore, these results suggest that Ni_3Al/GC and Ni_3Ga/HOPG may not operate via a Fischer-Tropsch-like mechanism, despite similarities in both reactants and products. H_2/D_2 studies of Fischer-Tropsch catalysis typically reveal an inverse isotopic effect on the order of $r_D/r_H = 1.2–1.6$, meaning that D_2 speeds up the multi-carbon product-generating reaction, though few catalysts exhibit normal kinetic isotope effects (i.e., $r_D/r_H < 1$).[27,28] To-date, no Fischer-Tropsch catalysts have failed to generate hydrocarbons altogether when in the presence of D_2 or D_2O.[29] Taken together, these results call into question the suggestion that Ni_3Al/GC and Ni_3Ga/HOPG electrocatalysts facilitate C2 and C3 product formation via a traditional Fischer-Tropsch catalytic mechanism.

Conclusions

Here, we have described how the synthesis and electrochemical testing of several Ni-G13 catalyst structures provided insight into the roles of the metals, carbon support, and catalytic mechanism in generating multi-carbon products. These Ni-G13 catalyst systems reduce CO_2 to C2 and C3 species only when in their intermetallic forms, signifying a synergistic role for the two metals and refuting the hypothesis that they perform isolated tasks during catalysis (e.g., CO_2 reduction to CO, CO reduction to higher-order products). Furthermore, the ability to generate higher-order products cannot be rescued by tuning the solid support on which non-mixed metals are deposited. During the experimental process, it was discovered that monoclinic Ga_2O_3 films situated on RVC are effective CO generators, reaching Faradaic efficiencies around 57%. A summary of the product distribution achieved using each electrocatalyst discussed herein is provided in Table S2.

Electrolysis experiments using D_2O-based electrolyte resulted in enhanced CO production for all catalysts studied, but the ability of Ni_3Al/GC and Ni_3Ga/HOPG to generate higher-order products was compromised. This extreme isotope effect lends insight into the

mechanism of CO_2 reduction on these catalysts, which have been said to exhibit Cu-like CO_2 reduction behavior. Reduction of CO must be rate-limiting given the CO accumulation recorded and, unlike many predictions regarding Cu catalysts, CO_2 reduction to C2 and C3 products might not proceed through a mechanistic route resembling Fischer-Tropsch catalysis.

These insights have several key implications for the study of bimetallic catalysts active in CO_2 electroreduction. At present, intermetallic catalysts seem more effective than non-mixed, two-metal species at generating higher-order products from CO_2. Development of non-alloyed systems seeking to combine separate reduction events at distinct metal sites will be even more challenging to develop, as the two metals will need to have compatible electrochemical conditions. Moreover, based on our isotopic experiments, it may be possible to elicit Cu-like CO_2 electroreduction activity without adopting what is presumed to be the dominant CO_2 reduction mechanism on Cu (i.e., Fischer-Tropsch). It would therefore be worthwhile to determine whether any Cu-based CO_2 reduction catalysts exhibit isotope effects similar the one described herein, as this could help distinguish critical pathway-product relationships for these popular catalyst materials.

Acknowledgements

The authors acknowledge financial support from the National Science Foundation under Grant No. CHE-1800400. In addition, ARP acknowledges funding from the National Science Foundation Graduate Research Fellowship Program under Grant No. DGE-1148900. Any opinions, findings, and conclusions expressed in this material are those of the authors and do not necessarily reflect the views of the National Science Foundation.

References

1 D. A. Torelli, S. A. Francis, J. C. Crompton, A. Javier, J. R. Thompson, B. S. Brunschwig, M. P. Soriaga and N. S. Lewis, *ACS Catalysis*, 2016, **6**, 2100–2104.
2 R. Kortlever, I. Peters, C. Balemans, R. Kas, Y. Kwon, G. Mul and M. T. M. Koper, *Chem. Commun.*, 2016, **52**, 10229–10232.
3 A. R. Paris and A. B. Bocarsly, *ACS Catalysis*, 2017, **7**, 6815–6820.
4 H. A. Hansen, C. Shi, A. C. Lausche, A. A. Peterson and J. K. Nørskov, *Phys. Chem. Chem. Phys.*, 2016, **18**, 9194–9201.
5 Z. P. Jovanov, H. A. Hansen, A. S. Varela, P. Malacrida, A. A. Peterson, J. K. Nørskov, I. E. L. Stephens and I. Chorkendorff, *Journal of Catalysis*, 2016, **343**, 215–231.
6 A. A. Peterson and J. K. Nørskov, *The Journal of Physical Chemistry Letters*, 2012, **3**, 251–258.
7 Z. W. Ulissi, M. T. Tang, J. Xiao, X. Liu, D. A. Torelli, M. Karamad, K. Cummins, C. Hahn, N. S. Lewis, T. F. Jaramillo, K. Chan and J. K. Nørskov, *ACS Catalysis*, 2017, 6600–6608.
8 K. Tran and Z. W. Ulissi, *Nature Catalysis*, 2018, **1**, 696–703.
9 Y. Li and Q. Sun, *Advanced Energy Materials*, 2016, **6**, 1600463.
10 A. Dutta, M. Rahaman, N. C. Luedi, M. Mohos and P. Broekmann, *ACS Catalysis*, 2016, **6**, 3804–3814.
11 M. Ma, K. Djanashvili and W. A. Smith, *Angewandte Chemie International Edition*, 2016, **55**, 6680–6684.
12 Y. Li, F. Cui, M. B. Ross, D. Kim, Y. Sun and P. Yang, *Nano Letters*, 2017, **17**, 1312–1317.
13 P. De Luna, R. Quintero-Bermudez, C.-T. Dinh, M. B. Ross, O. S. Bushuyev, P. Todorović, T. Regier, S. O. Kelley, P. Yang and E. H. Sargent, *Nature Catalysis*, 2018, **1**, 103–110.

14 S. Rasul, D. H. Anjum, A. Jedidi, Y. Minenkov, L. Cavallo and K. Takanabe, *Angewandte Chemie International Edition*, 2015, **54**, 2146–2150.
15 R. Kortlever, I. Peters, S. Koper and M. T. M. Koper, *ACS Catalysis*, 2015, **5**, 3916–3923.
16 A. R. Paris, A. T. Chu, C. B. O'Brien, J. J. Frick, S. A. Francis and A. B. Bocarsly, *Journal of The Electrochemical Society*, 2018, **165**, H385–H392.
17 Y. Hori, A. Murata and R. Takahashi, *Journal of the Chemical Society, Faraday Transactions 1: Physical Chemistry in Condensed Phases*, 1989, **85**, 2309–2326.
18 Y. Hori, R. Takahashi, Y. Yoshinami and A. Murata, *The Journal of Physical Chemistry B*, 1997, **101**, 7075–7081.
19 R. Kortlever, J. Shen, K. J. P. Schouten, F. Calle-Vallejo and M. T. M. Koper, *The Journal of Physical Chemistry Letters*, 2015, **6**, 4073–4082.
20 J. Wang, *Electrochimica Acta*, 1981, **26**, 1721–1726.
21 J. M. Friedrich, C. Ponce-de-León, G. W. Reade and F. C. Walsh, *Journal of Electroanalytical Chemistry*, 2004, **561**, 203–217.
22 Y. Hori, H. Wakebe, T. Tsukamoto and O. Koga, *Electrochimica Acta*, 1994, **39**, 1833–1839.
23 T. Sekimoto, M. Deguchi, S. Yotsuhashi, Y. Yamada, T. Masui, A. Kuramata and S. Yamakoshi, *Electrochemistry Communications*, 2014, **43**, 95–97.
24 K. J. P. Schouten, Y. Kwon, C. J. M. van der Ham, Z. Qin and M. T. M. Koper, *Chemical Science*, 2011, **2**, 1902.
25 K. J. P. Schouten, Z. Qin, E. P. Gallent and M. T. M. Koper, *Journal of the American Chemical Society*, 2012, **134**, 9864–9867.
26 C. K. Rofer-DePoorter, *Chemical Reviews*, 1981, **81**, 447–474.
27 C. S. Kellner and A. T. Bell, *Journal of Catalysis*, 1981, **67**, 175–185.
28 M. Ojeda, A. Li, R. Nabar, A. U. Nilekar, M. Mavrikakis and E. Iglesia, *The Journal of Physical Chemistry C*, 2010, **114**, 19761–19770.
29 S. Krishnamoorthy, M. Tu, M. P. Ojeda, D. Pinna and E. Iglesia, *Journal of Catalysis*, 2002, **211**, 422–433.

Table 1. Summary of materials characterization data comparing Ni_3Al/GC and Ni_3Ga/HOPG intermetallics with non-mixed 3Ni-Al/GC and 3Ni-Ga/HOPG. Bulk composition was determined by a combination of XRD and EDX, while surface composition was obtained from XPS analysis. Data for Ni_3Al/GC and Ni_3Ga/HOPG were reported previously.[3,16]

	Bulk		*Surface*	
Catalyst	**Ni**	**G13**	**Ni**	**G13**
Ni_3Al/GC	Ni_3Al (cubic)		Ni(II) oxides + Ni	Al_2O_3
3Ni-Al/GC	Ni (cubic)	Al_2O_3 (amorphous)	Ni(II) oxides + Ni	Al_2O_3
Ni_3Ga/HOPG	Ni_3Ga (cubic)		Ni(II) oxides + Ni	Ga_2O_3 + Ga
3Ni-Ga/HOPG	Ni (cubic)	Ga_2O_3 (monoclinic)	Ni(II) oxides + Ni	Ga_2O_3 + Ga

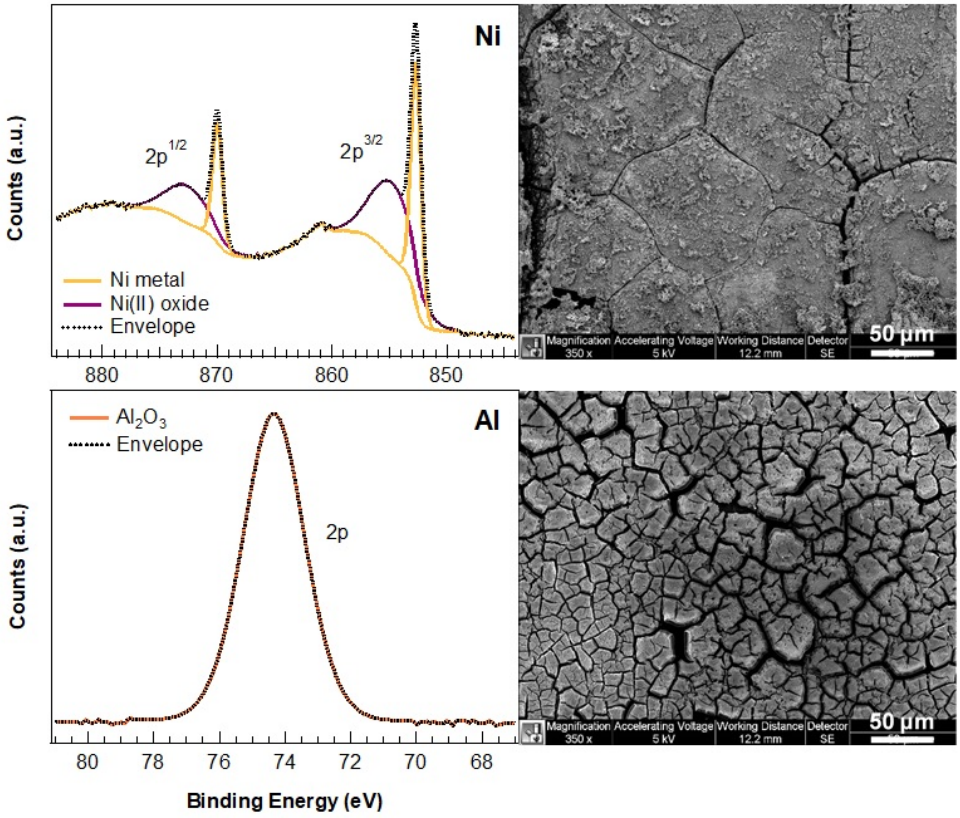

Figure 1. Surface characterization of 3Ni-Al/GC. XPS data (left) indicate that the surfaces of both the Ni and Al components are heavily oxidized. SEM imaging (right) suggests that both metal films on GC are comprised of relatively flat platelets. SEM images were acquired using a 5 keV electron beam.

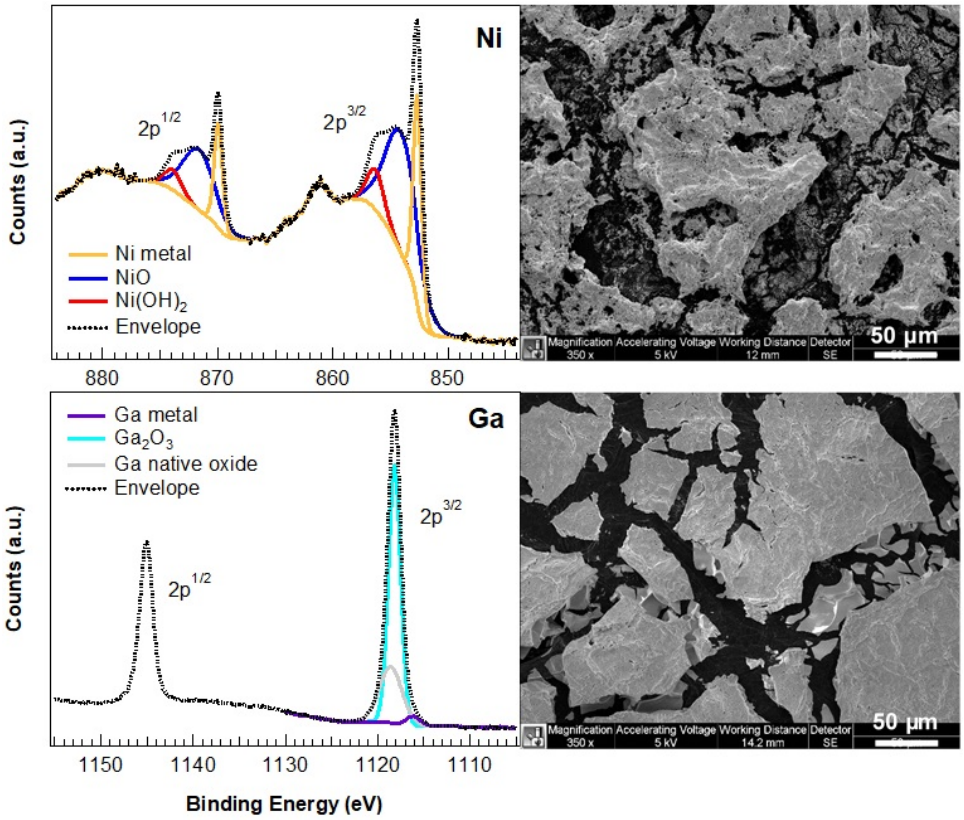

Figure 2. Surface characterization of 3Ni-Ga/HOPG. XPS data (left) indicate that the surfaces of both the Ni and Ga components are heavily oxidized. SEM imaging (right) shows that the Ni and Ga films on HOPG are made up of rough, non-uniform particles. SEM images were acquired using a 5 keV electron beam.

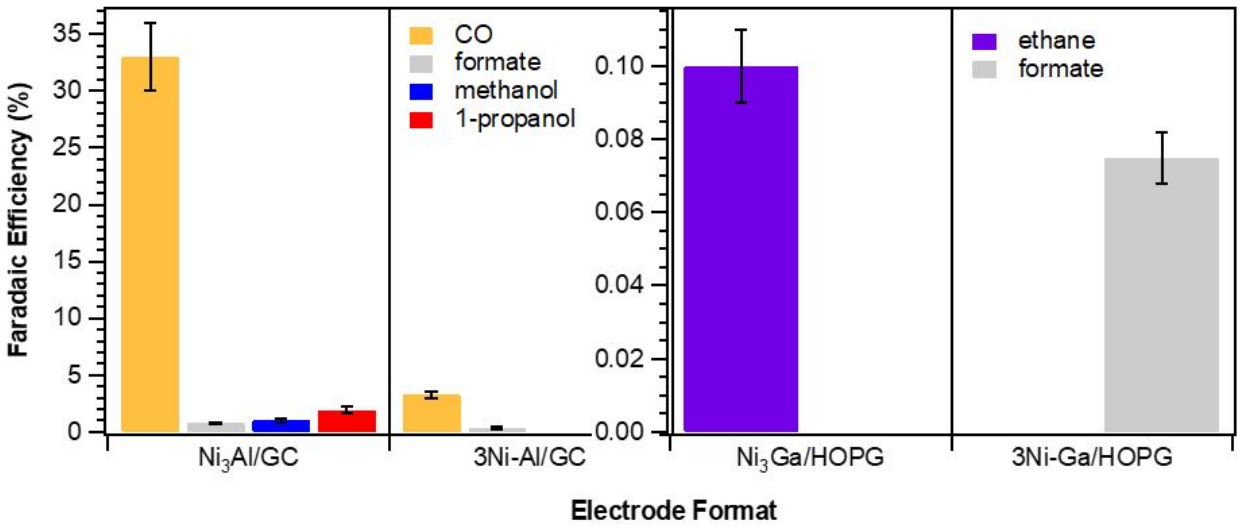

Figure 3. Distribution of CO_2 reduction products achieved using intermetallic and non-mixed Ni-G13 catalysts on carbon solid supports. Higher-order products could only be generated in the presence of Ni_3Al or Ni_3Ga intermetallic compounds.[3,16] Electrolysis experiments were conducted at –1.38 V vs. Ag/AgCl in pH 4.5, CO_2-saturated K_2SO_4 electrolyte.

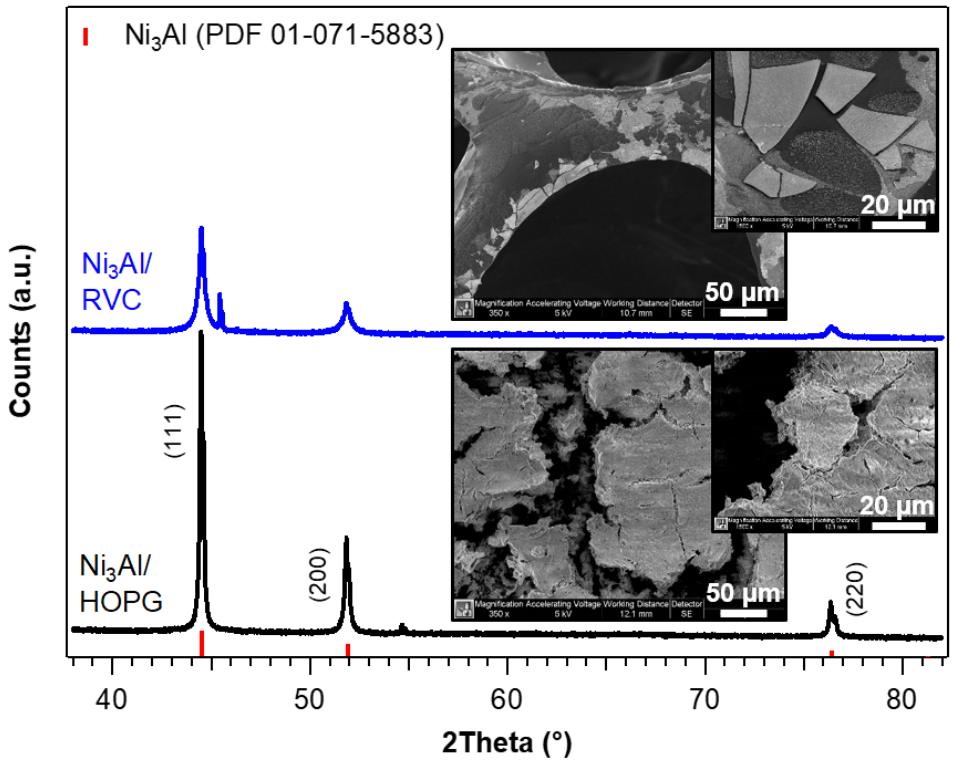

Figure 4. XRD patterns confirm synthesis of Ni_3Al on both RVC (blue; top) and HOPG (black; bottom) solid supports. Unmarked peaks are attributed to carbon. Inset SEM images indicate smooth platelet and rough particle morphologies for RVC- and HOPG-deposited Ni_3Al, respectively.

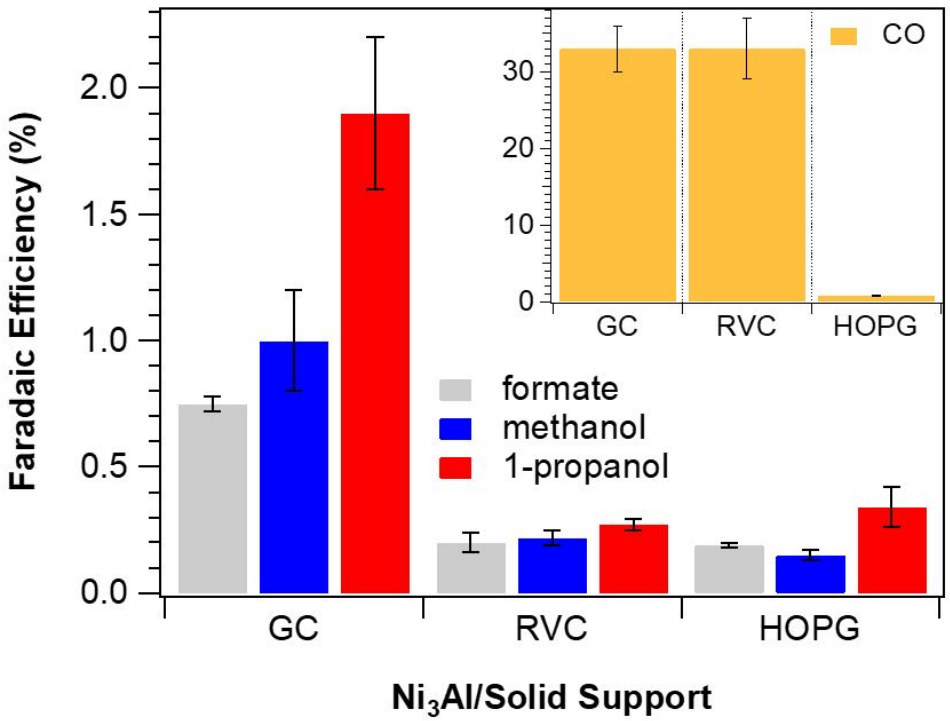

Figure 5. Faradaic efficiencies for CO_2 reduction products achieved using Ni_3Al films on different carbon solid supports. While the relative efficiencies of products vary, the product distribution remains the same irrespective of support choice. Ni_3Al/GC values were reported previously.[3] Electrolysis experiments were conducted at –1.38 V vs. Ag/AgCl in pH 4.5, CO_2-saturated K_2SO_4 electrolyte.

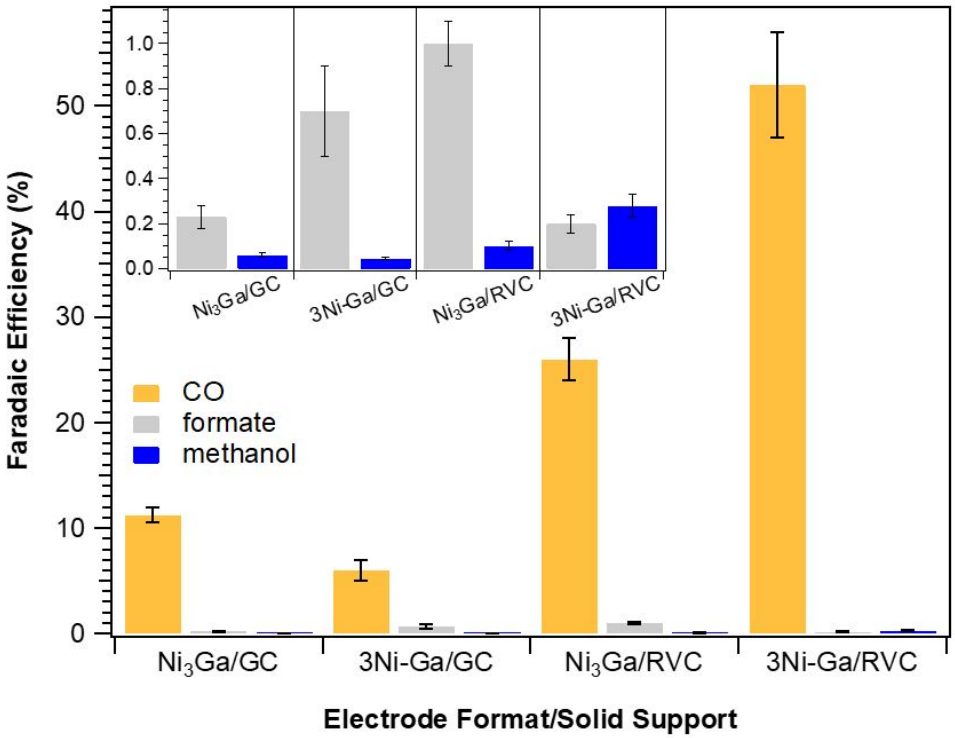

Figure 6. Faradaic efficiencies for CO_2 reduction products achieved using Ni_3Ga and non-mixed 3Ni-Ga films on GC and RVC solid supports, indicating that the intermetallic and non-mixed species exhibit the same product distribution. Ni_3Ga/GC and Ni_3Ga/RVC values were reported previously.[16] Electrolysis experiments were conducted at –1.38 V vs. Ag/AgCl in pH 4.5, CO_2-saturated K_2SO_4 electrolyte.

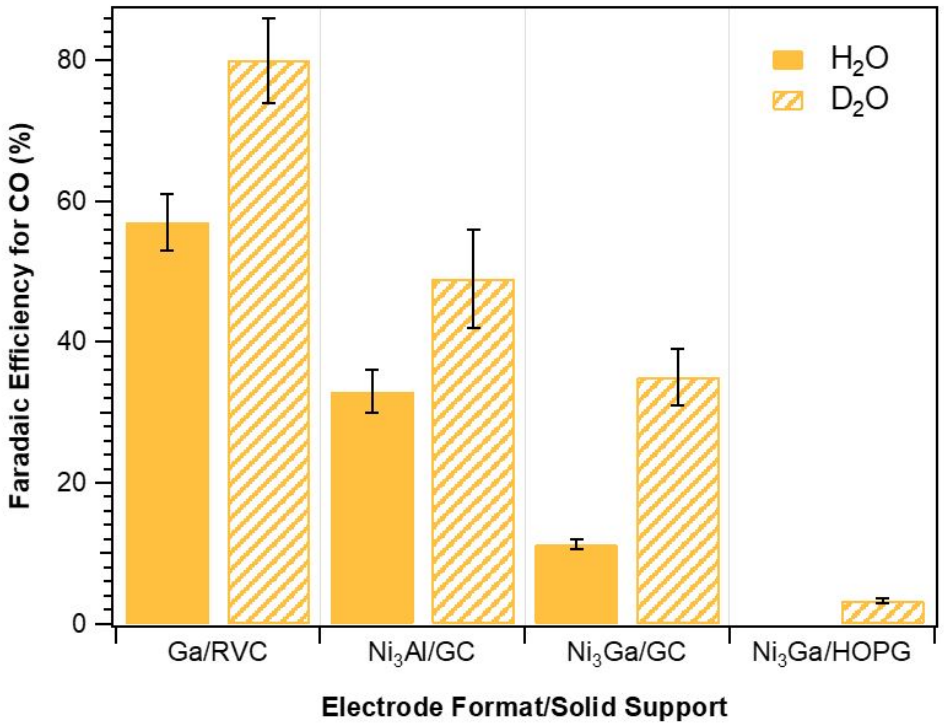

Figure 7. Faradaic efficiencies for CO achieved using different electrode-support combinations in H_2O- or D_2O-based electrolyte (0.1 M K_2SO_4). The D_2O environment consistently increased CO production and eliminated higher-order product generation where previously possible. Electrolysis experiments were conducted at –1.38 V vs. Ag/AgCl.

TOC figure